Electronic Supplementary Material (ESI) for Journal of Materials Chemistry A.

Defect and interlayer spacing engineering of vanadium selenide for boosting sodium-ion storage

Wang Feng,[‡a] Xia Wen,[‡a] Yanan Peng,[a] Luying Song,[a] Xiaohui Li,[a] Ruofan Du,[a] Junbo Yang,[a] Yulin Jiang,[a] Hui Li,[a] Hang Sun,[a] Ling Huang,[a] Jun He[b] and Jianping Shi[*a]*

[a]The Institute for Advanced Studies, Wuhan University, Wuhan 430072, China.
Email: jianpingshi@whu.edu.cn
[b]Key Laboratory of Artificial Micro- and Nano-structures of Ministry of Education, School of Physics and Technology, Wuhan University, Wuhan 430072, China
[‡]These authors contributed equally to this work.

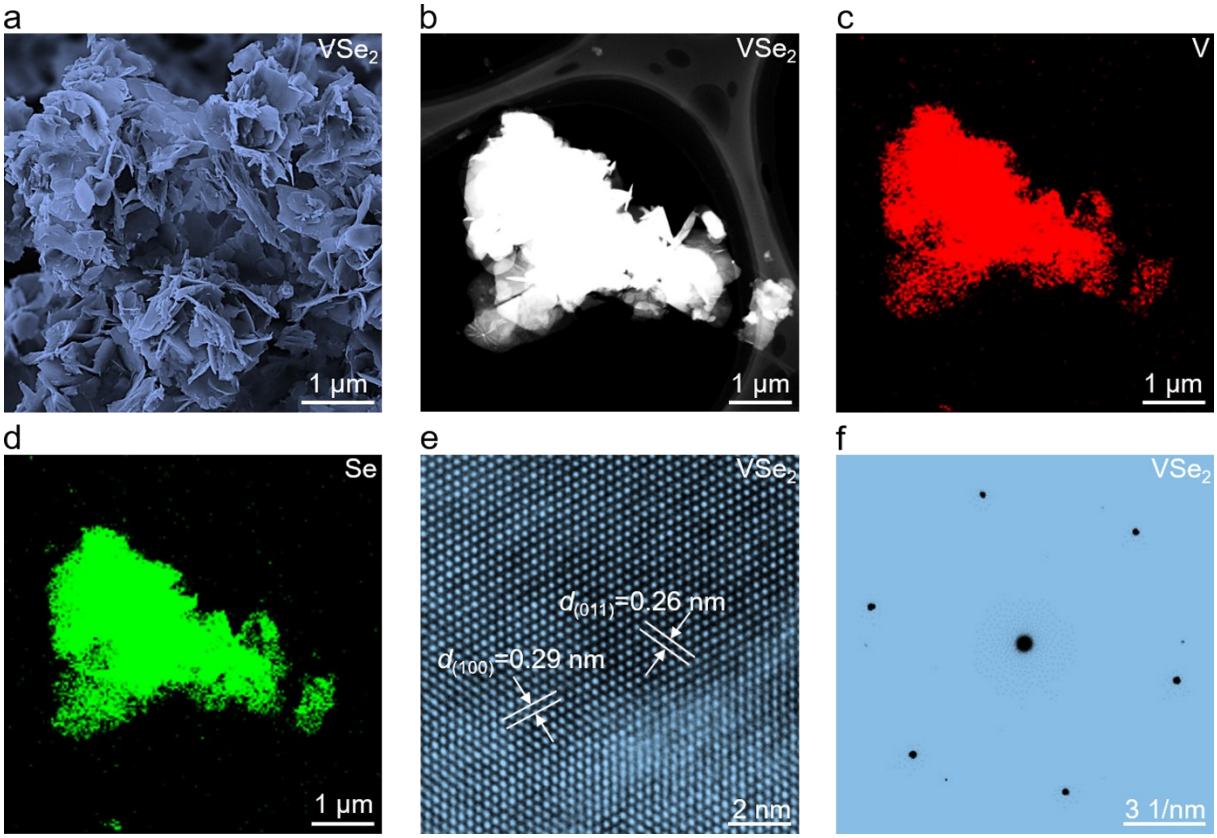

Fig. S1 Morphology and atomic structure characterization of as-grown pure VSe_2. (a) SEM image of pure VSe_2, showing its layered structure. (b) Low-magnification TEM image of pure VSe_2. (c,d) EDS maps of pure VSe_2, indicating the uniform distribution of V and Se elements. (e) Atomic-resolution TEM image of pure VSe_2, showing its high crystalline quality. (f) Corresponding selected area electron diffraction (SAED) pattern of pure VSe_2.

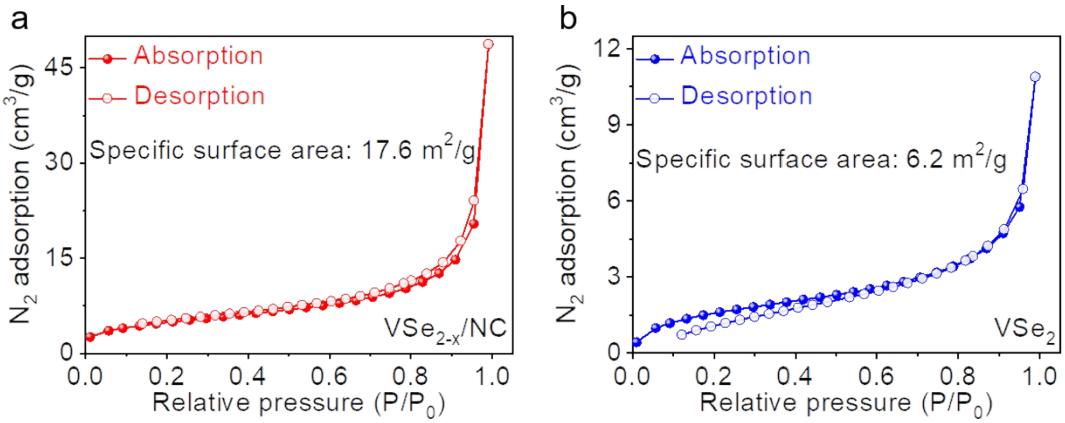

Fig. S2 Specific surface area determination of VSe_{2-x}/NC (a) and pure VSe_2 (b) by nitrogen adsorption/desorption isotherms. The specific surface areas of VSe_{2-x}/NC and pure VSe_2 are calculated to be 17.6 and 6.2 m^2/g, respectively.

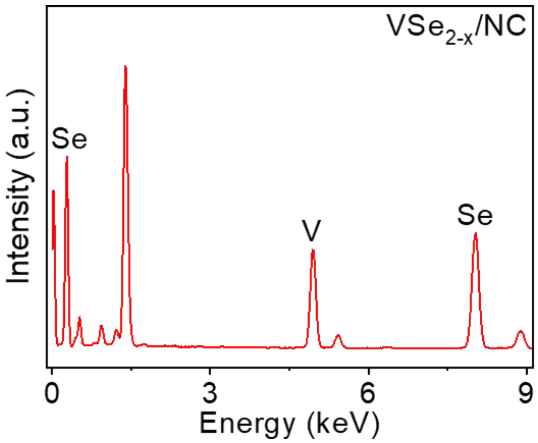

Fig. S3 EDS analysis of as-grown VSe_{2-x}/NC. The atomic ratio of V and Se is calculated to be 1:1.8, higher than the stoichiometric ratio of VSe_2, indicating the formation of Se vacancy in VSe_{2-x}/NC.

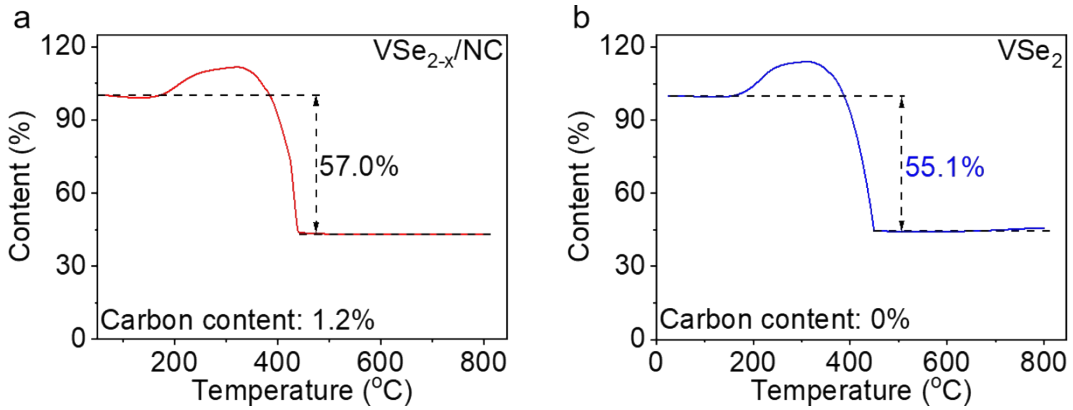

Fig. S4 Thermogravimetric analysis (TGA) curves of VSe_{2-x}/NC (a) and pure VSe_2 (b). The carbon contents of VSe_{2-x}/NC and pure VSe_2 are assessed to be 1.2% and 0%, respectively.

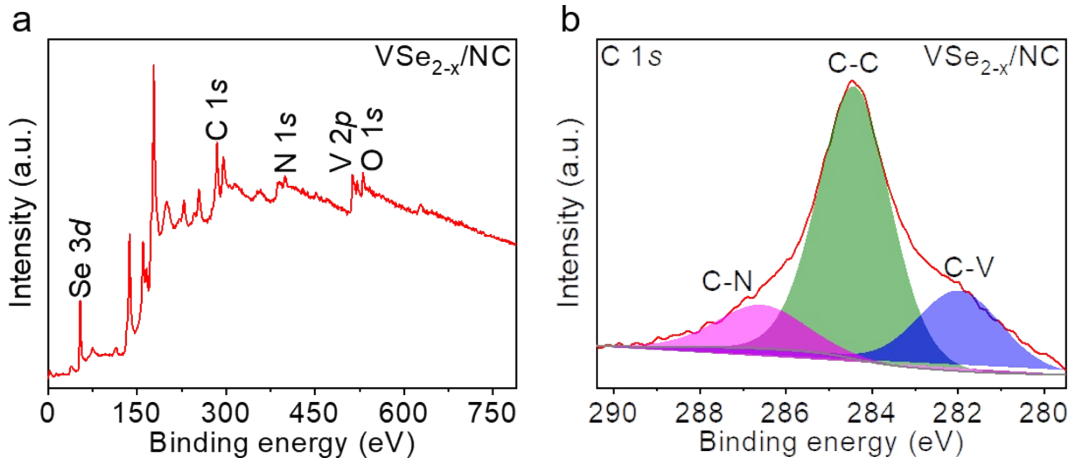

Fig. S5 XPS characterization of as-grown VSe_{2-x}/NC. (a) XPS spectrum acquired over a wide range of binding energies (0~780 eV). (b) High resolution XPS spectrum of C 1*s*. The binding energies of C-N, C-C, and C-V are located at 286.6, 284.4, and 282.0 eV, respectively.

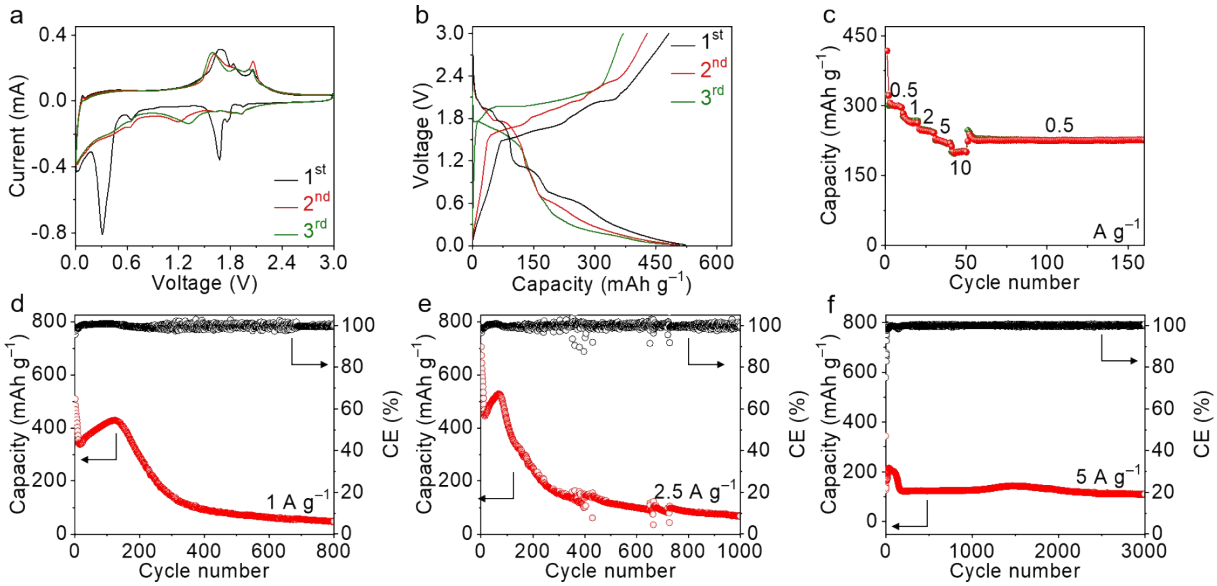

Fig. S6 Sodium-ion storage performances of pure VSe_2. (a) CV curves of pure VSe_2 in the first three cycles with a scan rate of 0.1 mV s^{-1}. (b) Galvanostatic charging/discharging curves of pure VSe_2 in the first three cycles at the current density of 1 A g^{-1}. (c) Rate capabilities of pure VSe_2 at different current densities. (d–f) Cycling performances of pure VSe_2 at the current densities of 1, 2.5, and 5 A g^{-1}, respectively.

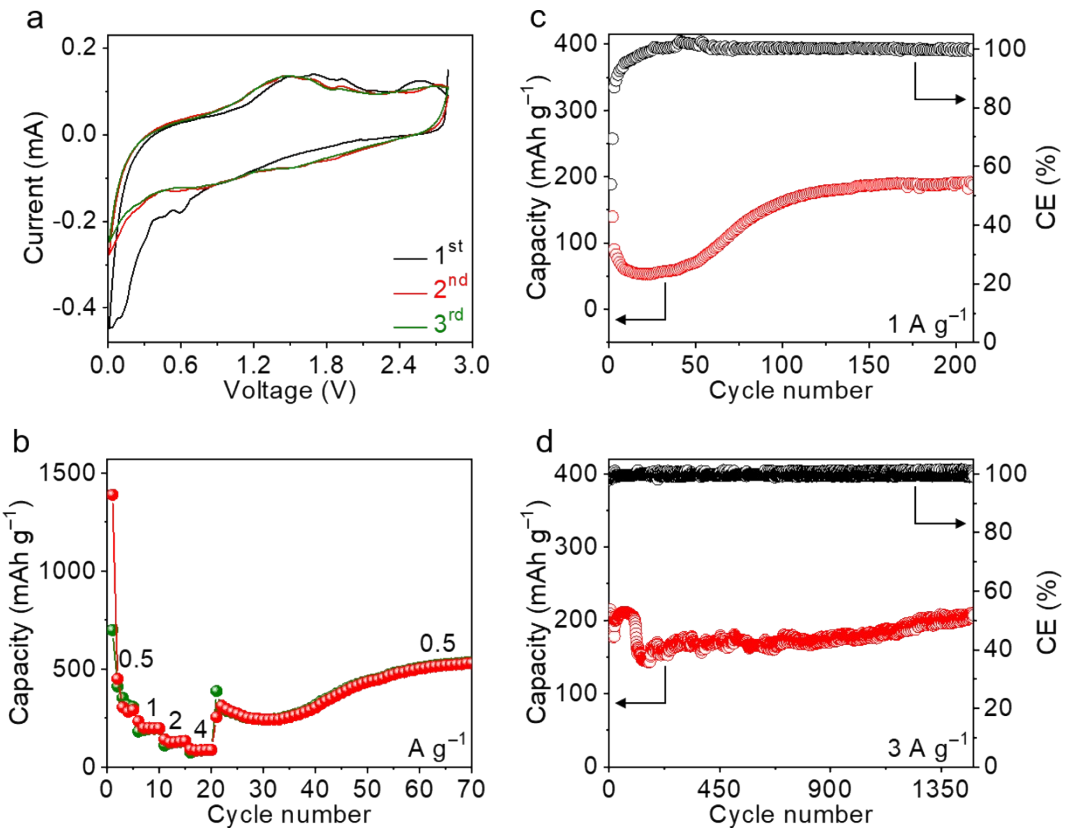

Fig. S7 Potassium-ion storage performances of VSe_{2-x}/NC. (a) CV curves of VSe_{2-x}/NC in the first three cycles with a scan rate of 0.1 mV s^{-1}. (b) Rate capabilities of VSe_{2-x}/NC at different current densities. (c,d) Cycling performances of VSe_{2-x}/NC at the current densities of 1 and 3 A g^{-1}, respectively.

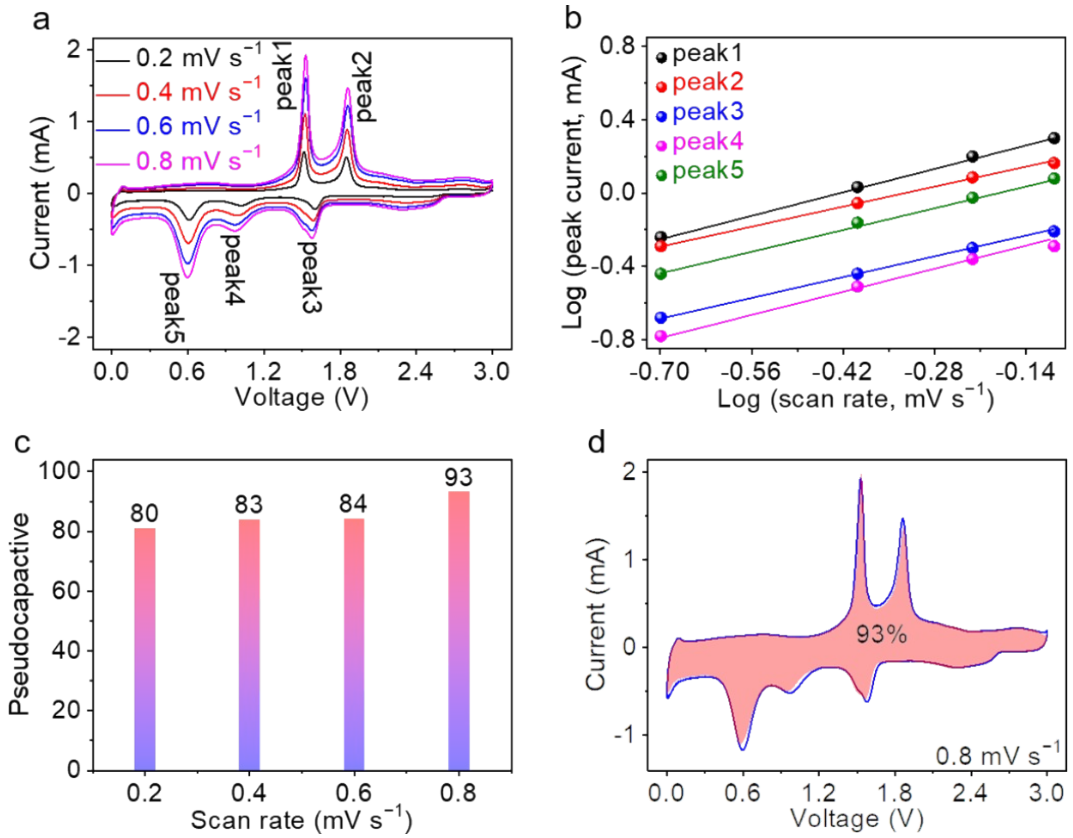

Fig. S8 Electrochemical kinetics of VSe_{2-x}/NC. (a) CV curves of VSe_{2-x}/NC at different scan rates. (b) The *b* values extracted from different scan rates. (c) Pseudocapacitive contributions of VSe_{2-x}/NC at different scan rates. (d) CV profile of VSe_{2-x}/NC with the pseudocapacitive contribution at a scan rate of 0.8 mV s^{-1}.

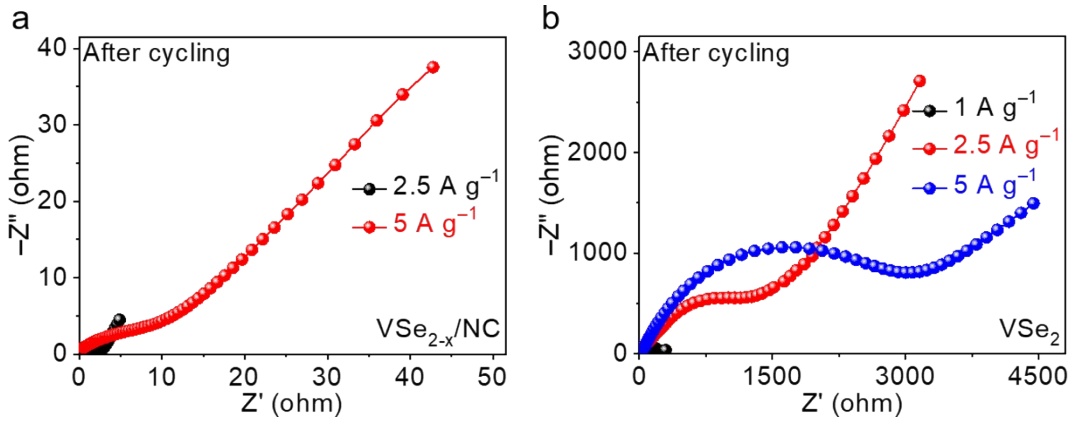

Fig. S9 EIS curves of VSe_{2-x}/NC (a) and pure VSe_2 (b) after the cycling tests at different current densities. The small resistance indicates the fast charge transfer in VSe_{2-x}/NC.

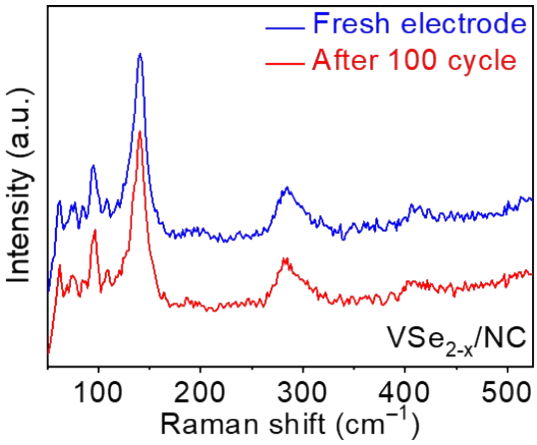

Fig. S10 Raman spectra of VSe_{2-x}/NC after different cycling numbers. The Raman characteristic peaks of VSe_{2-x} are still reserved, indicating its robust atomic structure.

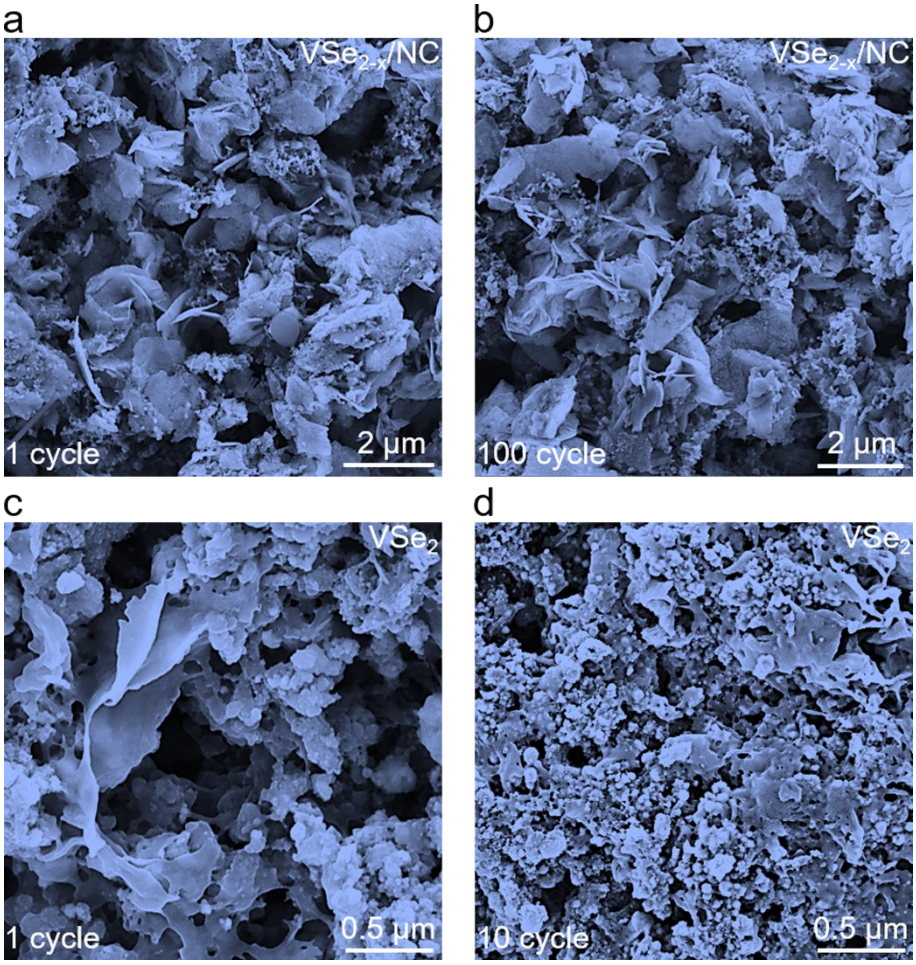

Fig. S11 Morphology characterization of VSe_{2-x}/NC and pure VSe_2 after cycling tests. (a,b) SEM images of VSe_{2-x}/NC after 1 and 100 cycles. (c,d) SEM images of pure VSe_2 after 1 and 10 cycles.

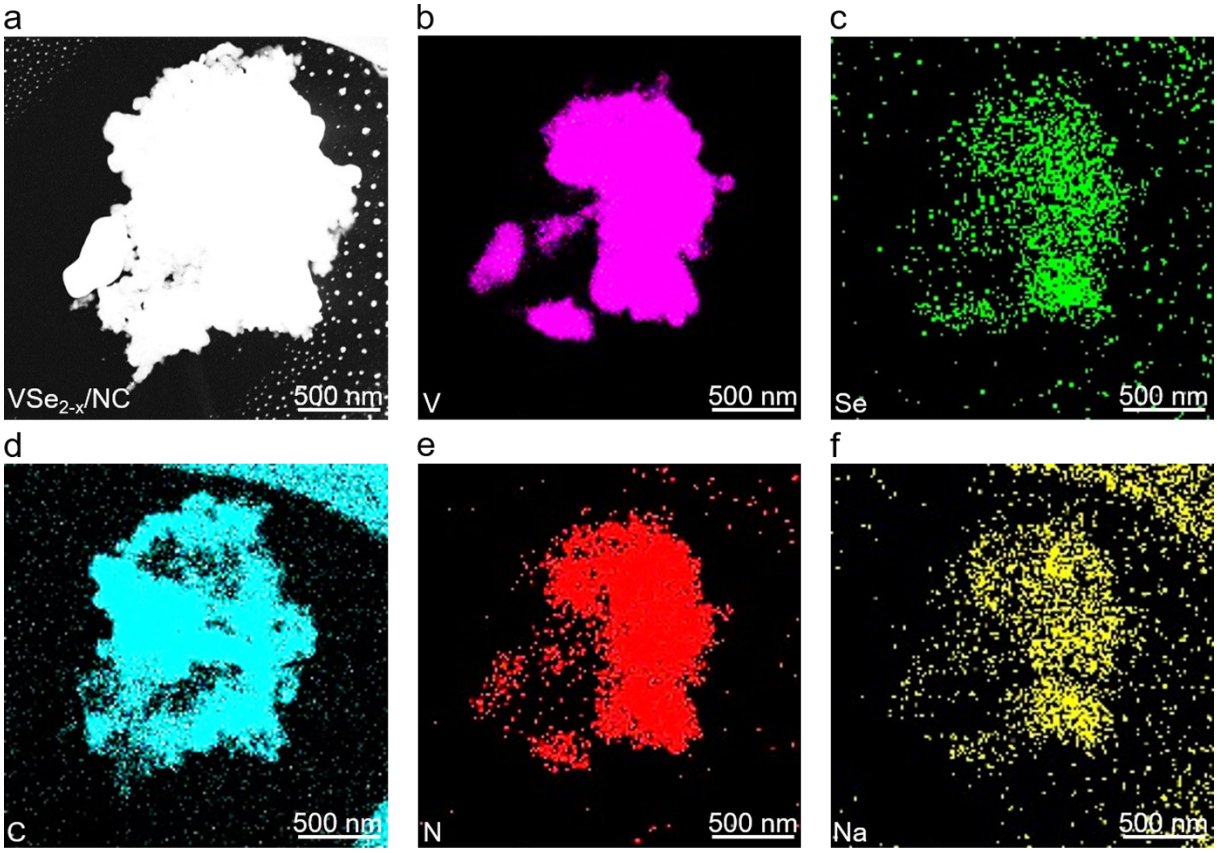

Fig. S12 Morphology and element distribution characterization of VSe_{2-x}/NC after discharging to 0.01 V. (a) Low-magnification TEM image of VSe_{2-x}/NC after discharging to 0.01 V. (b−f) Corresponding EDS maps of VSe_{2-x}/NC, indicating the uniform distribution of V, Se, C, N, and Na elements.

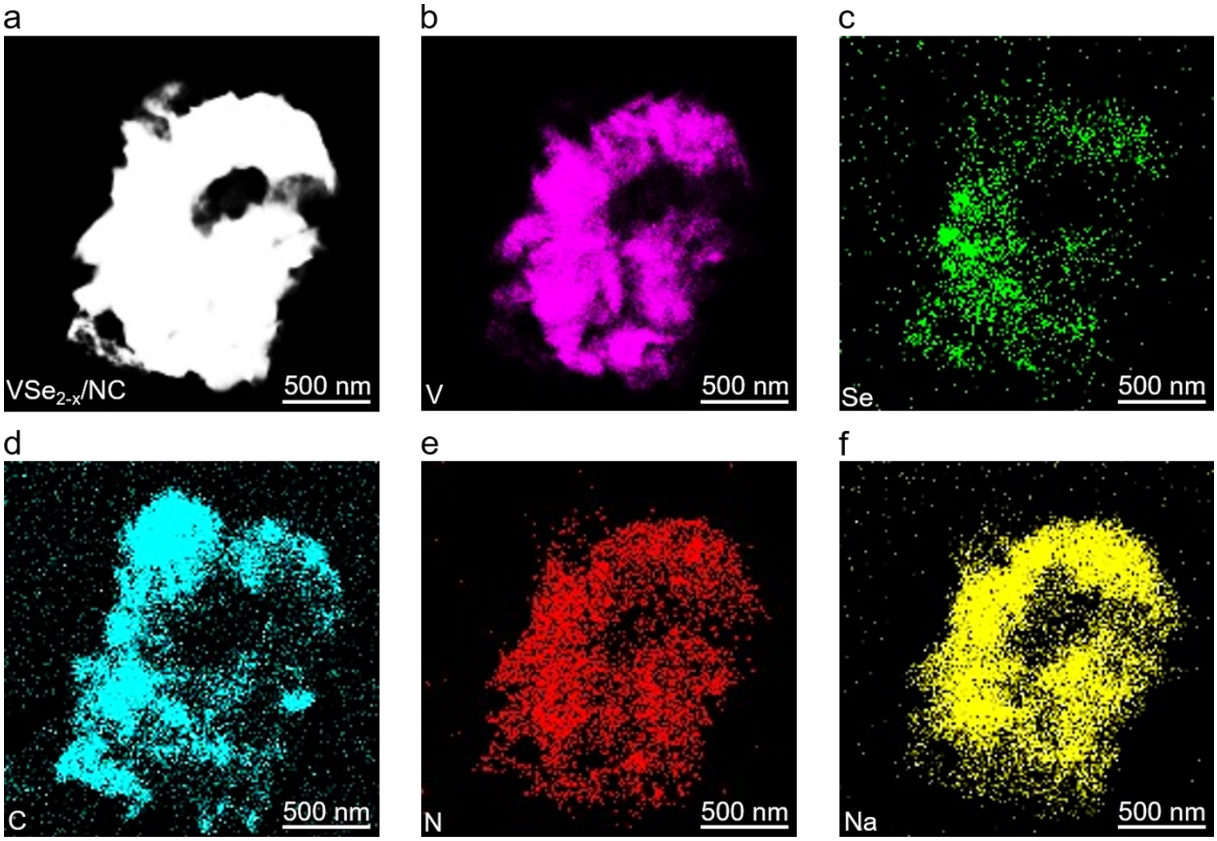

Fig. S13 Morphology and element distribution characterization of VSe_{2-x}/NC after charging to 3.0 V. (a) Low-magnification TEM image of VSe_{2-x}/NC after charging to 3.0 V. (b−f) Corresponding EDS maps of VSe_{2-x}/NC, indicating the uniform distribution of V, Se, C, N, and Na elements.

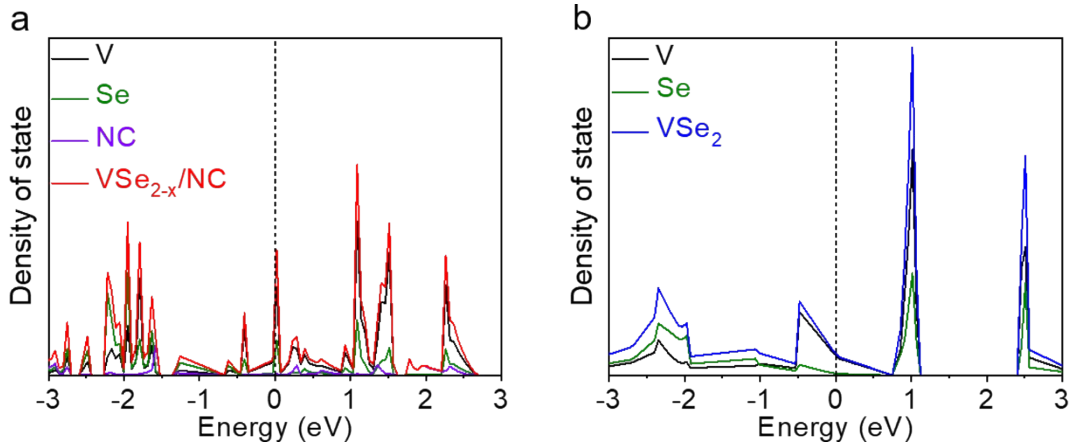

Fig. S14 Electronic structures of VSe_{2-x}/NC (a) and pure VSe_2 (b). The high density of state (DOS) is observed at the Fermi level of VSe_{2-x}/NC comparing to pure VSe_2, which enhances the conductivity and accelerates the electron/ion transport.

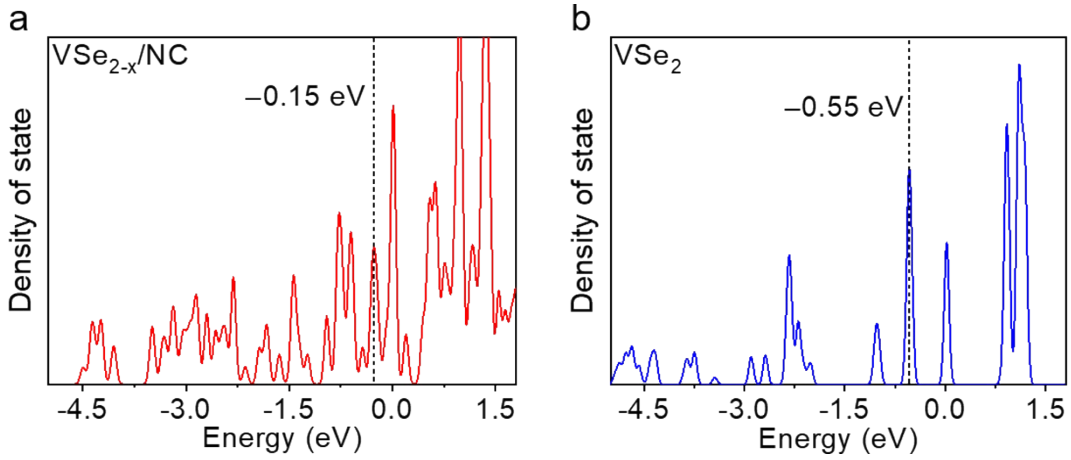

Fig. S15 DFT calculations of the V *d* band centers for VSe_{2-x}/NC (a) and pure VSe_2 (b). The upshift of V *d* band center is observed for VSe_{2-x}/NC, which increases the metal-adsorbate interaction.

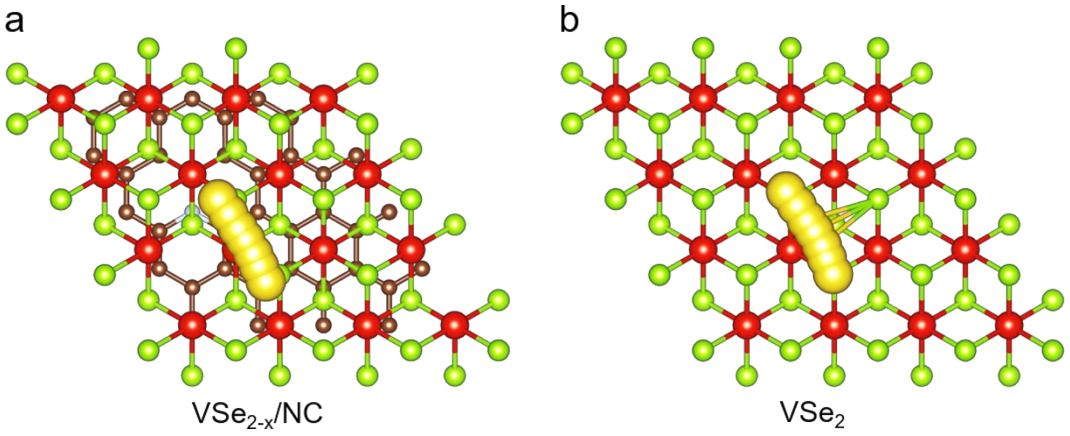

Fig. S16 DFT calculations of Na^+ diffusion pathways on VSe_{2-x}/NC (a) and pure VSe_2 (b). A relatively low migration barrier is obtained for VSe_{2-x}/NC.

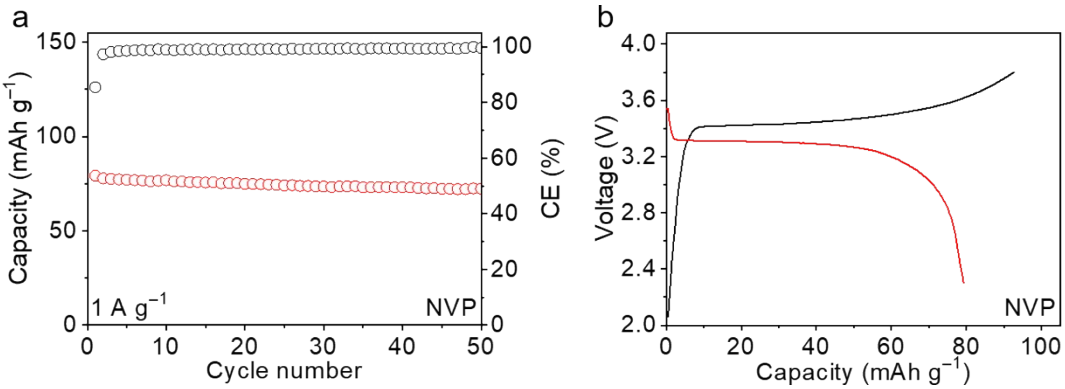

Fig.S17 Electrochemical performances of NVP cathodes. (a) Cycling performance of NVP at the current density of 1 A g^{-1}. (b) Galvanostatic charging/discharging curves of NVP in the first cycle at the current density of 1 A g^{-1}.

Table S1. The capacity comparison of VSe_{2-x}/NC with other vanadium-based chalcogenides

Material	Current density (A g^{-1})	Capacity (mAh g^{-1})	Ref.
VSe_2@PPy	1	333.6	1
	2	270.9	
	3	266.8	
	5	262.9	
	10	260.0	
VSe_2@rGO	0.05	365.0	2
	0.1	330.0	
	0.2	313.0	
	0.5	270.0	
	1	239.0	
	2	208.4	
	5	163.8	
VS_2	0.1	175.0	3
	0.2	150.0	
	0.5	130.0	
	1	100.0	
VS_4@rGO	0.2	552.0	4
	0.5	471.0	
	1	422.0	
	2	340.0	
	5	238.0	
	10	173.0	
	20	123.0	
VS_2 nanosheet	0.1	250.0	5
	0.5	205.0	
	1	200.0	
	2	195.0	
	5	180.0	
	10	170.0	
	15	160.0	
	20	150.0	

V_5S_8@C	0.2	548.0	6
	0.5	508.0	
	1	464.0	
	2	407.0	
	5	304.0	
	10	190.0	
V_3S_4	0.2	481.0	7
	0.5	424.0	
	1	388.0	
	2	348.0	
V_3S_4@CNF	0.1	400.0	8
	0.2	380.0	
	0.5	345.0	
	1	305.0	
	2	265.0	
	5	200.0	
	10	185.0	
VSe_{2-x}/NC	0.5	584.4	This work
	1	523.8	
	2	475.9	
	5	448.7	
	10	432.1	

1. Y. H. Yi, X. Du, Z. P. Zhao, Y. Liu, H. Guan, X. F. Liu, X. D. Pei, S. Zhang and D. Li, *ACS Nano*, 2022, **16**, 7772–7782.
2. X. Zhang, Q. He, X. M. Xu, T. Xiong, Z. T. Xiao, J. S. Meng, X. P. Wang, L. Wu, J. H. Chen and L. Q. Mai, *Adv. Energy Mater.*, 2020, **10**, 1904118.
3. S. Z. Wang, F. Gong, S. Z. Yang, J. X. Liao, M. Q. Wu, Z. Q. Xu, C. Chen, X. F. Yang, F. P. Zhao, B. Wang, Y. S. Wang and X. L. Sun, *Adv. Funct. Mater.*, 2018, **28**, 1801806.
4. R. M. Sun, Q. L. Wei, J. Z. Sheng, C. W. Shi, Q. Y. An, S. J. Liu and L. Q. Mai, *Nano Energy*, 2017, **35**, 396–404.
5. C. H. Yang, X. Ou, X. H. Xiong, F. H. Zheng, R. Z. Hu, Y. Chen, M. L. Liu and K. Huang, *Energy Environ. Sci.*, 2017, **10**, 107–113.
6. Y. J. Zhang, J. L. Li, L. Ma, H. B. Li, X. T. Xu, X. J. Liu, T. Lu and L. K. Pan, *Chem. Eng. J.*, 2022, **427**, 130936.
7. G. Yao, P. Niu, Z. Q. Li, Y. Xu, L. Z. Wei, H. L. Niu, Y. Yang, F. C. Zheng and Q. W. Chen, *Chem. Eng. J.*, 2021, **423**, 130229.
8. Y. K. Wu, H. Chen, L. C. Zhang, Q. L. Li, M. W. Xu and S.-J. Bao, *Inorg. Chem. Front.*, 2019, **6**, 2935–2943.